



HAL
open science

Nanoscale Metallic Iron for Environmental Remediation: Prospects and Limitations

Chicgoua Noubactep, Sabine Caré, Richard Crane

► **To cite this version:**

Chicgoua Noubactep, Sabine Caré, Richard Crane. Nanoscale Metallic Iron for Environmental Remediation: Prospects and Limitations. *Water, Air, and Soil Pollution*, 2012, 3 (223), pp.1363-1382. 10.1007/s11270-011-0951-1 . hal-00674132

HAL Id: hal-00674132

<https://enpc.hal.science/hal-00674132>

Submitted on 5 Mar 2012

HAL is a multi-disciplinary open access archive for the deposit and dissemination of scientific research documents, whether they are published or not. The documents may come from teaching and research institutions in France or abroad, or from public or private research centers.

L'archive ouverte pluridisciplinaire **HAL**, est destinée au dépôt et à la diffusion de documents scientifiques de niveau recherche, publiés ou non, émanant des établissements d'enseignement et de recherche français ou étrangers, des laboratoires publics ou privés.

28 **1 Introduction**

29 The development of new methods and materials for environmental remediation is a real
30 challenge for the scientific community. Such technologies will only be adopted by industry if
31 they can exhibit marked improvements in efficiency, affordability or eco-compatibility
32 compared to conventional techniques. The use of metallic iron (Fe^0) in subsurface reactive
33 permeable barriers has been identified as such a technology [1-4]. Since this discovery almost
34 20 years ago, extensive research of $\text{Fe}^0/\text{H}_2\text{O}$ system has been performed in an attempt to
35 understand the controlling mechanisms behind the remediation of redox-amenable
36 contaminant species using Fe^0 -based materials [5-14]. Two different tools are commonly used
37 to optimise the efficiency of Fe^0 for aqueous contaminant removal: (i) reducing the particle
38 size of Fe^0 down to the nanoscale (nano- Fe^0) [15,16], and (ii) using bimetallic systems
39 [17,18]. In recent years there has been considerable interest into combining the two methods
40 [19-23].

41 Since the original proof of concept study into the application of nano- Fe^0 for water treatment
42 at Lehigh University, USA [15], research within this field has boomed. On April 23th 2011, a
43 search at “**Science Direct**” using key words “*nanoscale*” and “*zerovalent iron*” yielded 208
44 peer-reviewed articles in 6 selected journals (Table 1). The same search at “**Environmental**
45 **Science and Technology**” resulted in 157 articles. According to Table 1, 59 articles have
46 already been published in the first quarter of 2011 in the 7 selected journals. This clearly
47 demonstrates the interest within academia for this technology.

48 In recent years, several review articles and critical views on nano- Fe^0 for environmental
49 remediation have been published [20, 24-40]. However, the original discussion on the
50 suitability of nano- Fe^0 for in-situ field applications [25] has not been satisfactorily addressed
51 [28,36]. Moreover, a recent comparison between field applications of Fe^0 of different particle
52 sizes (nm, μm , and mm) for field applications has clearly demonstrated the superiority of mm-
53 Fe^0 (average efficacy 97 %) [11]. The decreasing order of reactivity was mm- Fe^0 (97 %) >

54 $\mu\text{m-Fe}^0$ (91 %) > nano- Fe^0 (65 %). Expectably, the lower efficiency of nano- Fe^0 is due their
55 high reactivity [25,34]. Therefore, the question arises on the fundamental necessity to further
56 increase the reactivity of nano- Fe^0 by using a noble metal combination.

57 **1.1 The problem**

58 Nano- Fe^0 technology for environmental remediation was introduced as an alternative to the
59 conventional Fe^0 walls mostly for inaccessible aquifers [27,41]. The very small particle size
60 of nano- Fe^0 (1–100 nm) would allow the material to penetrate deep into soil networks
61 [11,12,20,39,40,42].

62 Due to the exponential relationship between specific surface area (SSA) and radius ($R = d/2$)
63 of a perfectly spherical object ($\text{SSA} = 4\pi R^2$), as a rule, a decrease in Fe^0 particle size increases
64 the surface area per gram by up to 3 orders of magnitude [22,29]. In other words, the inverse
65 relationship between Fe^0 particle size and reactivity is due to a greater density of reactive sites
66 on the particle surface at smaller scale. The following three claims have been made with
67 regard to the use of nano- Fe^0 for aqueous contaminant removal (ref. [12] and ref. therein): (i)
68 some aqueous contaminant species that have been proven as unsuccessful for remediation
69 using $\mu\text{m-Fe}^0$ and mm-Fe^0 can be effectively removed using nano- Fe^0 , (ii) nano- Fe^0 can be
70 used for more rapid degradation of contaminants, and (iii) the formation of some undesirable
71 by-products during remediation using $\mu\text{m-Fe}^0$ and mm-Fe^0 can be avoided by using nano- Fe^0 .
72 Such processes whilst correct are all linked to the greater reactivity nano- Fe^0 possesses due to
73 its size (reactive surface area). When performed in conditions without a large nano- Fe^0
74 stoichiometric excess, e.g. a system analogous to the environment, it may prove that such
75 claims will be unfounded [21,34,36,43,44].

76 An undisputed drawback with regards to the use of nano- Fe^0 for environmental applications is
77 their strong tendency to aggregate and adhere to solid surfaces [11,12,20,27,30,39,40,43].
78 Karn et al. [20] listed some parameters that influence nano- Fe^0 adsorption onto soil and
79 aquifer materials: (i) the surface chemistry of soil and Fe^0 particles, (ii) the groundwater

80 chemistry (e.g., ionic strength, pH and presence of natural organic matter), and (iii) the
81 hydrodynamic conditions (pore size, porosity, flow velocity and degree of mixing or
82 turbulence). Several methods have been developed for the stabilization of nano-Fe⁰ particles
83 over the past decade and proven efficient to sustain the reactivity of nano-Fe⁰ [11,12,20,43].
84 One factor that has been overlooked, however, is the impact volumetric expansion has on the
85 mobility of (i) residual Fe⁰, (ii) primary corrosion products (Fe^{II} and H₂) and contaminants.
86 The volume of any corrosion product (Fe hydroxide or oxide) is higher than that of the
87 original metal (Fe⁰). The ratio between the volume of expansive corrosion product and the
88 volume of iron consumed in the corrosion process is called "rust expansion coefficient" (η)
89 [45-47]. Volumetric corrosion products are likely to: (i) contribute to porosity loss, (ii) impact
90 the retention of contaminants and transformation products, and (iii) increase the particle
91 agglomeration.

92 Another area of heightened research is with regard to the determining the toxicity of nano-
93 Fe⁰, with mixed results reported [12,48]. For example, Barnes et al. [49] reported minimal
94 change to the structure of a river water community due to the addition of nano-Fe⁰, while
95 Diao and Yao [50] reported nano-Fe⁰ particles as highly cytotoxic towards both gram-positive
96 and gram-negative bacteria species.

97 While taking into account all known influencing parameters, the following seven features
98 have to be systematically studied in order to optimise the general applicability of this
99 technique [12,20,51]: (i) mobility changes due to nano-Fe⁰ volumetric expansion during
100 corrosion, (ii) the bioavailability of Fe⁰ and corrosion products (Fe^{II}/Fe^{III} species, H/H₂), (iii)
101 the ecotoxicity of Fe⁰ and its corrosion products, (iv) the bioaccumulation of Fe⁰ and its
102 corrosion products, (v) the translocation potential of nano-Fe⁰, (vi) the long-term reactivity of
103 nano-Fe⁰ particles, and (vii) the speciation, persistence and fate of contaminants and their
104 transformation products. A major contributing factor to the latter point is that little is known

105 (compared to permeable reactive barrier technologies) about the extent contaminants are
106 removed via size exclusion using nano-Fe⁰.

107 Only when all seven “operational drivers” have been determined can the global community
108 have full faith in the technology.

109 **1.2 Objectives of the study**

110 The present communication is focused on the “field persistence” or reactive “life span” of
111 nano-Fe⁰ particles. For in-situ applications a keen understanding of nano-Fe⁰ reactive fate is
112 essential for effective and prudent site clean-up. The knowledge of which is likely to largely
113 underpin decisions as to the (i) the choice of material selected, (ii) the mechanism of
114 application and, (iii) the strategy (if any) for repeated treatments.

115 In the current work a multidisciplinary approach is used to analyse the relationship between
116 nano-Fe⁰ reactivity and its performance for in-situ field applications. The discussion is based
117 on the contemporary knowledge of the mechanism of aqueous contaminant removal by Fe⁰
118 [52-54]. Much of the impetus for this work has come from the work of Noubactep and Caré
119 [34], who have challenged the concept that nano-Fe⁰ is a strong reducing agent for
120 contaminant reductive transformation.

121 **2 Nanoscale metallic iron or environmental remediation**

122 To date, nano-Fe⁰ particles have been reported as largely successful for water and soil
123 treatment [11,31,32,55,56]. A wide variety of redox-amenable organic and inorganic species
124 and non-reducible species (e.g. Cd, Zn) have been efficiently treated. Similar to μm and mm -
125 Fe⁰, adsorption is considered important only for non-reducible species [52-54, 57-60]. For
126 example, Boparai et al. [59] reported that heavy metals are either reduced (e.g. Cu²⁺, Ag²⁺) at,
127 or directly adsorbed (e.g. Zn²⁺, Cd²⁺) onto the Fe⁰ surface. They further argued that “the
128 controlling mechanism is a function of the standard redox potential of the contaminant”.
129 Recent work has however challenged this concept [36,54], which is explained below.

130 **2.1 Contaminant reduction by nano-Fe⁰**

131 The chemical reaction between Fe^0 and redox-amenable aqueous species is considered to
132 involve three steps: (i) direct electron transfer from Fe^0 at the metal surface or through a
133 conductive oxide film on Fe^0 (direct reduction), (ii) catalyzed hydrogenolysis by the H/H_2
134 (indirect reduction mechanism 1), and (iii) reduction by Fe^{II} species resulting from Fe^0
135 corrosion (indirect reduction mechanism 2). In this constellation, H_2 is supposed to result
136 from H_2O reduction during anoxic iron corrosion [22,61]. However, evidence exists in the
137 literature, e.g. Stratmann and Müller [62], that even under external oxic conditions, Fe^0 is
138 oxidized by H_2O (or more precisely by H^+) and O_2 by Fe^{II} (Table 2). Despite the significant
139 reaction rate exhibited by nano- Fe^0 due to its high surface area, such processes are considered
140 to occur (discounting any quantum size effects) independent of particle size.

141 Table 2 summarizes the half reactions for the aqueous oxidation of Fe^0 under both anoxic and
142 oxic conditions. Thermodynamically, the major cathodic reaction depends on the availability
143 of molecular O_2 ($E^0 = 0.81$ V). In the absence of O_2 , Fe^0 is oxidized by H^+ ($E^0 = 0.00$ V). It
144 can therefore be stated that the rate of Fe^0 oxidation is dictated by the concentration of
145 dissolved O_2 , H^+ and H_2O in proximity to Fe^0 surfaces. Le Chatelier's principle also states that
146 the consumption of Fe^{II} (via oxidation to Fe^{III}) will also result in an increase in Fe^0 oxidation.

147 The electrode potential of the redox couple $\text{Fe}^{\text{II}}/\text{Fe}^0$ is -0.44 V, a value which is independent
148 of the particle size (nm, μm or mm). The value -0.44 V is considered largely unchanged due
149 to the presence of alloying materials (e.g. low alloy steel, bimetallic systems).

150 As a consequence, statements including “*nano- Fe^0 are more reactive than $\mu\text{m-Fe}^0$ and mm-*
151 *Fe^0 ” are misleading; as the reactivity of Fe^0 (discounting quantum size effects), is independent
152 of the particle size. Any enhanced reactivity reported is likely to be due to the significantly
153 high surface area of nano- Fe^0 compared to other forms. A second statement “*bimetallic nano-*
154 *Fe^0 is more reactive than monometallic nano- Fe^0 ” is also a qualitative statement, as the
155 reactivity of the materials depends on numerous factors associated with the materials
156 synthesis route and varies depending on the chemistry of the chosen alloying metal. Ideally,**

157 comparisons should be made versus standard reference materials using established standard
158 experimental protocols [63], which once established, will significantly improve the design of
159 future field applications.

160 **2.2 Limitations of the nano-Fe⁰ technology**

161 The efficiency of nano-Fe⁰ for aqueous contaminant reduction faces some key issues for in-
162 situ applications in porous media. These challenges include: (i) the strong tendency of
163 aggregation/agglomeration, (ii) the rapid settlement on subsurface solid phases, (iii) the
164 porosity and permeability loss of porous media [23,35,64,65]. Aggregation and settlement
165 limit nano-Fe⁰ transport through porous media. Porosity and permeability loss limit nano-Fe⁰
166 transport to target contaminants. It was demonstrated that nano-Fe⁰ may travel only a few
167 centimetres in porous media from the injection position under typical groundwater conditions
168 [11,12,30,66]. Accordingly, recent efforts have been made to (i) increase the porosity of
169 porous media, (ii) mechanically increase the distribution of nano-Fe⁰, and/or (iii) chemically
170 modify nano-Fe⁰ for improved aqueous mobility in porous networks.

171 **2.3 Improving the efficiency of the nano-Fe⁰ systems**

172 **2.3.1 Dispersion agents**

173 Methods to improve the aqueous mobility of nano-Fe⁰ have received the greatest research
174 interest. It has been determined that the key to improving particle mobility is found in
175 modifying their surface properties such that the nano-Fe⁰ have significantly improved
176 colloidal stability and a commensurate reduction in the likelihood of adherence to mineral
177 surfaces. Several synthetic methods are now available to produce more mobile nano-Fe⁰.
178 Efficiently tested dispersants include anionic surface chargers (e.g. polyacrylic acid), non-
179 ionic surfactants, starch, and oil [23,67-70].

180 **2.3.2 Bimetallic combinations**

181 In recent years, noble metals have been used to increase the reactivity of monometallic nano-
182 Fe⁰ [21,23,71-73]. As mentioned above, this appears counterintuitive as nano-Fe⁰ is already

183 high reactivity due to its size [15,26,29,42] and is unstable during synthesis, storage and
 184 application [69]. This chemical instability has been documented as a key reason for the
 185 observed lower efficiency exhibited by nano-Fe⁰ systems compared to μm and mm-Fe⁰ [11].
 186 Accordingly, it is questionable whether further enhancing the reactivity of nano-Fe⁰, e.g. by
 187 plating with more noble elements, may be of any benefit. The reactivity of nano-Fe⁰ will be
 188 discussed in the next section on the basis of mathematical modelling.

189 **3 Significance of increased reactivity**

190 **3.1 The problem**

191 The increased Fe⁰ reactivity from mm to nm size should be better characterized. The relative
 192 reactivity of four different materials is discussed on the basis of 1 kg Fe⁰: one nm-Fe⁰ (d₀ = 25
 193 nm), one μm-Fe⁰ (d₀ = 25 μm), and two mm-Fe⁰ (d₀ = 250 and 1000 μm). Calculations for the
 194 number particles (N) in 1 kg of each material and the number of layers (N') in each particle
 195 are made after the Eq. (1) and Eq. (2) presented in details elsewhere [9,74].

$$196 \quad N = \frac{M}{\rho_{\text{Fe}} \cdot 4/3\pi \cdot R_0^3} \quad (1)$$

197

$$198 \quad N' = 2 \cdot [4/3(\pi R_0^3)]/a^3 \quad (2)$$

199 where M is the mass of Fe⁰ (here 1 kg), ρ_{Fe} is the specific weight of Fe (7,800 kg/m³), R₀ is
 200 the initial radius of the Fe particle (d = 2*R₀) and a the lattice parameter (a = 2.866 Å).

201 The results are summarized in Table 3. It can be seen that the number of layers of Fe⁰ in
 202 individual particles varies from 87.2 for nano-Fe⁰ to more than 3*10⁶ for mm-Fe⁰ (d = 1 mm).
 203 In the meantime, the number of particles in 1 kg decreased from 1.96*10¹⁸ for nano-Fe⁰ to
 204 only 3.1*10⁴ for mm-Fe⁰. The ratio of the number of Fe⁰ layers in each particle to the number
 205 of Fe⁰ layers in nano-Fe⁰ varies from 1 to 4*10⁴. This ratio corresponds to the relative time (τ)
 206 as defined later (section 3.2). On the other hand, the ratio of the number of particles in 1 kg of
 207 nano-Fe⁰ to the number of particles in the same mass of each other materials varies from 1 to

208 6.4×10^{13} . These results are summarized in Fig. 1. Instead of the mass of Fe^0 , the number of
209 electrons released by the conversion of Fe^0 to Fe^{II} is used to assess the kinetics of Fe^0
210 consumption. This is discussed in the next section.

211 **3.2 Relative corrosion kinetics of Fe^0 materials**

212 For the discussion in this section, uniform corrosion for spherical particles is assumed.
213 Individual particles corrode independently until material depletion. It is further assumed for
214 simplicity that individual layers corrode with the same kinetics independent of particle size (d
215 $= 2 \cdot R_0$). The latter assumption is conservative as larger particles react slower than smaller
216 [24,29,61]. With these assumptions, a relative time (τ) can be defined while taking the time
217 for the corrosion of the smallest particle (here 87.2 layers of nano- Fe^0) or $t_{\infty, \text{nano}}$ as unit.

$$218 \quad \tau = t/t_{\infty, \text{nano}} \quad (3)$$

219 Accordingly, one unit of time corresponds to the time to nano- Fe^0 depletion. Remember that
220 all 1.96×10^{18} particles in the 1 kg of nano- Fe^0 simultaneously corrode with the same kinetics.
221 The results of the calculations are presented in Fig. 2. From Fig. 2a and Tab. 3 it can be seen
222 that after nano- Fe^0 depletion, the material with 1000 μm (or 1 mm) diameter will still react for
223 more than 3×10^4 times longer than the time necessary for nano- Fe^0 depletion ($\tau = 4 \times 10^4$, see
224 Tab. 3). Fig. 2b shows that the mm- Fe^0 with 250 μm diameter is depleted after about
225 $10^4 \cdot t_{\infty, \text{nano}}$.

226 Based on the assumptions above, the service life of a nano- Fe^0 particle can be estimated.
227 Table 4 summarizes the results of such estimations while varying the service life of a 1 mm
228 Fe^0 particle from 5 to 40 years. This assumption is based on the fact that conventional Fe^0
229 walls are supposed to function for several decades (here up to 4 decades). Results show (Tab.
230 4) that the maximum life-span of a nano- Fe^0 is about 8.8 hours (less than one day). In other
231 words, following approximately 9 hours from subsurface deployment it is suggested that all
232 nano- Fe^0 would be reactively exhausted. The success of this is dependent on three key

233 factors: (i) the hydrodynamic conditions: pore size, porosity, flow velocity and degree of
234 mixing or turbulence, (ii) the water chemistry and the affinity of nano-Fe⁰ and its
235 transformation products to the soil materials, and (iii) the reactivity of Fe⁰.

236 It is certain, that the dynamic process of transformation of concentric layers of Fe⁰ atoms to
237 concentric layers of iron (hydr)oxides can not be linear [34]. In fact, effects similar to "case
238 hardening" for food- and wood-drying will lead to "surface hardened layers" [75, 76] leading
239 to differential kinetics/extents of Fe⁰ passivation for different particle size ranges. In other
240 words, the extend of restricted corrosion rates through resulting surface hardened layers will
241 be different for nm-, μm- and mm-Fe⁰. Bearing this in mind, the very short relative life-span
242 of a nano-Fe⁰ estimated above will be used for the discussion in this work. It is certain that
243 "case hardening"-like effects will prolong this hypothetical life-span to some days or weeks.

244 **3.3 Extent of iron corrosion from Fe⁰ materials**

245 A discussion as to the extent of Fe⁰ consumption is limited in the present section to $\tau = 1$ or
246 $t_{\infty, \text{nano}}$. It is considered for simplification that the sole iron corrosion product is Fe₃O₄. The
247 corresponding coefficient of volumetric expansion is $\eta_{\text{Fe}_3\text{O}_4} = 2.08$ (Eq. 4) [46]. Using $\rho =$
248 M/V , the volume of Fe corresponding to 1 kg Fe⁰ is calculated as 127.0 mL (V_0). This is the
249 initial volume of Fe⁰ (V_0). Following corrosion, this volume is partly or totally consumed.
250 The volume (ΔV) corresponding to the volume of pores occupied by the volumetric expansion
251 of corrosion products can be estimated.

252 Assuming that the coefficient of volumetric expansion (η) ("rust expansion coefficient" or
253 "specific volume") [45-47] of the reaction products is:

$$254 \quad \eta = V_{\text{oxide}}/V_{\text{Fe}} \quad (4)$$

255 where V_{oxide} is the volume of the reaction product and V_{Fe} the volume of the parent Fe⁰.

256 The volume ΔV characterizing the extent of porosity loss due to volumetric expansion is
257 given by Eq. 5:

258
$$\Delta V = (\eta - 1) * V_{\text{consumed Fe}} \quad (5)$$

259
$$\Delta V = V_{\infty} - V_0 = v*(\eta_{\text{Fe}_3\text{O}_4} - 1)*V_0 \quad (5a)$$

260 Where $V_{\text{consumed Fe}}$ is the volume of consumed Fe^0 at time t_{∞} , V_0 is the volume occupied by the
 261 initial Fe^0 particles and v ($v \leq 1$) is the fraction of the initial amount of Fe^0 (1 kg) which has
 262 reacted at $t_{\infty, \text{nano}}$. V_{∞} is the total volume occupied by residual Fe^0 and in-situ formed corrosion
 263 products. t_{∞} corresponds to nano- Fe^0 depletion (25 nm in this section). In the discussion on
 264 the reactivity at nano-scale, t_{∞} corresponds to the depletion of the material with 10 nm
 265 diameter (section 4).

266
$$V_{\infty} = \eta * V_{\text{consumed Fe}} + (V_0 - V_{\text{consumed Fe}}) \quad (6)$$

267
$$V_{\infty} = V_0 [1 + v*(\eta_{\text{Fe}_3\text{O}_4} - 1)] \quad (6a)$$

268 The volumetric expansion (ΔV , Eq. 5) can be characterized as percent of the initial volume
 269 (V_0) using Eq. (7):

270
$$\Delta V (\%) = 100*v*(\eta_{\text{Fe}_3\text{O}_4} - 1) \quad (7)$$

271 Table 5 summarizes the results. It is shown that at $\tau = 1$ (nano- Fe^0 depletion), a volume
 272 augmentation of 108 % has occurred in the nano- Fe^0 system, with volume augmentations in
 273 all other systems lower than 0.5 %. This clearly shows that the porosity of the subsurface will
 274 be significantly influenced by nano- Fe^0 at t_{∞} . Remember that 100 % reactive exhaustion of
 275 nano- Fe^0 is predicted to occur by approximately 9 hours time. During this same period the
 276 porosity loss due to expansive iron corrosion is likely to be negligible for all other Fe^0 particle
 277 size fractions. Calculations for Akageneite $\beta\text{-FeOOH}$ ($\eta_{\text{FeOOH}} = 3.48$) as sole corrosion
 278 products shows that $V_{\infty, \text{nano}} = 448.7$ mL, $\Delta V = 320.5$ mL or 250.4 %. The examples of Fe_3O_4
 279 (anoxic) and FeOOH (oxic) demonstrate the crucial importance of the nature of formed
 280 corrosion products for the discussion of the extent of porosity loss.

281 Another important aspect of Fe^0 consumption is given by the number of moles of Fe^0 that
 282 have been oxidized (Tab. 5). Assuming contaminant reduction, Tab. 5 shows that after $\tau = 1$,

283 35.71 moles of electrons have been released in the nano-Fe⁰ system but less than 0.11 moles
284 in all other systems. In other words, up to 35.71 moles of electrons are available for
285 contaminant reduction per kg nano-Fe⁰ within a few hours of reaction (< 9 hours). But what
286 proportion of the electrons produced would reach the contaminant within this period? That is
287 the major question to be answered for the further development of the nano-Fe⁰ technology for
288 in-situ applications.

289 **4 Reactivity of nano-Fe⁰ materials**

290 The presentation until now has discussed the reactivity of nano-Fe⁰ in comparison to larger
291 scale Fe⁰. Section 4 will focus only on the nanoscale size fraction ($d \leq 100$ nm). Equations 1-7
292 will be used and the particle size will vary from 10 to 100 nm. As stated above t_{∞} is for a
293 nano-Fe⁰ of 10 nm diameter and the reaction proceeding until 100 % reactive exhaustion has
294 been achieved.

295 **4.1 Fe⁰ reactivity at nanoscale**

296 Table 6 summarizes the results of calculations for the number of Fe⁰ particles and number of
297 layers of Fe⁰ in each nano-Fe⁰. It is shown that 1 kg of the material with $d = 100$ nm contains
298 1000 times more particles than a material of $d = 10$ nm.

299 Table 6 also shows that the maximum value of the relative time (τ) is 10 (or 10^1). This is more
300 practical for graphical representations than situations where nano-Fe⁰ are compared to larger
301 particles ($t \leq 10^4$). The physical significance of τ is more important, it means that if a nano-
302 Fe⁰ with a diameter of 10 nm depletes after 2 days, the material with a diameter 100 nm will
303 deplete after 20 days. For field applications the selection of the particle size to be used should
304 be dictated by site specific characteristics. Which diameter could quantitatively reach the
305 contaminants before depletion? And what fraction of the material will have already oxidized
306 on the path? What is the impact of this oxidation on the transport of nano-Fe⁰ in the porous
307 aquifer? These are some key questions to be answered in order to give this possibly very
308 efficient technology a scientific basis.

309 Fig. 3 summarizes the evolution of the volumetric expansion in all 5 nano-Fe⁰ systems. It can
310 be seen from Fig. 3a that the smallest material (d = 10 nm) experiences the 108 % volumetric
311 expansion within a short time ($\tau = 1$) while the larger materials (d = 100 nm) needs 10 more
312 time for the same expansion. Accordingly, beside the question whether the material will reach
313 the contaminant under site specific conditions, the question has to be answered how the
314 volumetric expansion will impact the aquifer porosity (and permeability).

315 Fig. 3b compares the variation of the volumetric expansion for two different iron corrosion
316 products, Fe₃O₄ and FeOOH, which are considered the most likely products in anoxic and
317 oxic aquifers respectively. It also shows that when designing a nano-Fe⁰ injection strategy,
318 however, the availability of oxidizing species (e.g. MnO₂, O₂) must also to be taken into
319 account. Fig. 3a shows that under both conditions the trend of porosity loss is similar but the
320 extent is proportional to the coefficient of volumetric expansion (η). In particular, at $\tau = 1$, the
321 system with the material d = 10 nm experiences 250 % volumetric expansion under oxic
322 conditions and only 110 % under anoxic conditions. As a result the kinetics of more rapid Fe⁰
323 corrosion in an oxygen-rich environment must also be considered for an effective treatment
324 strategy.

325 **4.2 Fe⁰ reactivity of nano-bimetallics**

326 The reactivity of monometallic nano-Fe⁰ can be improved by combining it with a noble metal.
327 Assuming α ($\alpha > 1$) the coefficient of reactivity enhancement, the relation between the
328 relative time of a bimetallic system ($\tau_{Fe/M}$) and that of a non plated metal (τ_{Fe}) is given by Eq.
329 6:

$$330 \quad \tau_{Fe} = \alpha * \tau_{Fe/M} \quad (8)$$

331 To characterize the impact of plating on nano-Fe⁰, the material with the largest size (d = 100
332 nm) will be plated by three hypothetical metals (M⁰₁, M⁰₂ and M⁰₃) to yield a reactivity factor
333 of 2.5 (for Fe⁰/M⁰₁), 5 (for Fe⁰/M⁰₂) and 10 (for Fe⁰/M⁰₃). The considered α values of ($\alpha \leq 10$)

334 are realistic and even conservative. In fact, reported reactivity enhancement is essentially
 335 larger [22,77]. For example, Zhuang et al. [77] reported that palladized nano-Fe⁰ promoted
 336 the dehalogenation kinetics for polybrominated diphenyl ethers by orders of magnitude equal
 337 to 2, 3 and 4 ($\alpha \geq 100$). The results of the calculations for the four systems ($d = 10$ nm) are
 338 summarized in Fig. 4. The system with $d = 10$ nm is represented for comparison. It can be
 339 seen that system Fe⁰/M₃⁰ ($d = 100$ nm) is as reactive as Fe⁰ ($d = 10$ nm). Given that the
 340 reactivity of nano-Fe⁰ ($d = 100$ nm) could already significantly been too high in some
 341 situations, the results from Fig. 4 strongly question the suitability of plating at nano-scale.
 342 Accordingly, while the application of bimetallic Fe⁰ is definitively useful at μ m- and mm-
 343 scale, its usefulness at nano-scale is likely inappropriate. It can also be noted that by increasing
 344 the reactivity of the material the rate at which volumetric pore clogging also increases. As a
 345 consequence it should be acknowledged that there exists a conceptual play-off between
 346 increased reaction rate and increased porosity loss, the impact of which will vary depending
 347 on the physiochemical conditions of each contaminated site.

348 **4.3 Characterizing the process of reactivity loss**

349 To better characterize the process of porosity loss due to the volumetric expansion of nano-
 350 Fe⁰, the evolution of the porosity of a sand column filled with nano-Fe⁰ will be discussed as
 351 volumetric expansion proceeds. A laboratory column with a height h ($h = 75.0$ cm) and
 352 diameter D ($D = 5.0$ cm) is composed of spherical sand particles ($d = 5.0$ mm). The
 353 compactness of the column is ideally $C = 0.64$ [9,74]. The pore volume is given by Eq. 9:

$$354 \quad V_{\text{pore}} = V * (1 - C) \quad (9)$$

355 where V is the apparent volume of the sand column ($V = h * \pi * D^2/4$).

356 It is supposed that the nano-Fe⁰ particles fill the inter-granular porosity of the sand column
 357 V_{pore} without modifying the compactness C and the apparent volume V of the sand column.

358 The residual porosity of the sand column (V'_{pore}) is given by Eq. 10:

$$359 \quad V'_{\text{pore}} = V*(1-C) - V_0 \quad (10)$$

360 where V_0 is the volume of the Fe particles.

361 The evolution of the residual porosity (V'_{pore}) as nano-Fe⁰ particles undergo volumetric
362 expansive corrosion is considered by introducing the specific volume (η) of the reaction
363 products according to Eq. 11:

$$364 \quad V'_{\text{pore}} = V^*(1 - C) - (V_0 - V_{\text{consumed Fe}}) - \eta * V_{\text{consumed Fe}} \quad (11)$$

$$365 \quad V'_{\text{pore}} = V^*(1 - C) - V_0 - (\eta - 1) * V_{\text{consumed Fe}} \quad (11a)$$

366 where $V_{\text{consumed Fe}}$ is the volume of nano-Fe⁰ particles which is consumed at a given time.

367 Equations 9 through 11 are very useful to design reactive zone. However, they are limited to
368 describe the initial (V_{pore}) and a final conditions (V'_{pore}) regardless on the nature of iron
369 corrosion products and the kinetics of the process.

370 Using a sand column comparable to one of those used by Moraci and Calabrò [78] and 1 kg of
371 nano-Fe⁰, the process of pore filling (porosity loss) can be better characterized. For simplicity
372 nano-Fe⁰ considered as transported by a biodegradable dispersant which does not significantly
373 contribute to porosity loss. As shown in section 3.3, 1 kg of nano-Fe⁰ occupies a volume of
374 127 mL. The initial pore volume of the sand column calculated after Eq. 9 is 530.36 mL (100
375 % porosity), i.e. a capacity for approximately 4.17 kg of nano-Fe⁰. Filling the initial pore
376 volume of the sand column (530.36 mL) with 1 kg of nano-Fe⁰ (127.00 mL) yields a 23.9 %
377 porosity loss (Tab. 7). This, however, does not take into account the expansive nature of iron
378 during oxidative corrosion.

379 Using the 8 possible iron corrosion products documented by Caré et al. [46] and their
380 respective coefficient of volumetric expansion ($2.08 \leq \eta \leq 6.40$), the extent of porosity loss is
381 calculated and summarized in Table 7. The results show that the residual volume of pores
382 (V'_{pore}) decreases with increasing η values and is zero for Fe(OH)₃ and Fe(OH)₃.3H₂O (100
383 % porosity loss). Ferrihydrite (Fe(OH)₃.3H₂O) is the largest known iron corrosion products.
384 In other words, depending on environmental conditions as little as 1 kg of nano-Fe⁰ could
385 clog the tested column. Although this discussion considers the nature of the corrosion

386 products, there are other important factors which must be considered. The negative values (-
387 3.04 and -282.4 mL) corresponds to the mass of Fe⁰ which will not oxidized because of lack
388 of space for expansion [9,74].

389 The extent of porosity loss (ΔV in %) given in Tab. 7 assumes uniform distribution of nano-
390 Fe⁰ in the whole column. This is, however, not a very good field representation. For example,
391 if 1 kg of nano-Fe⁰ ($V_0 = 127$ mL) is uniformly distributed only in the first third of the column
392 ($V_{\text{pore}}^{1/3} = 176.8$ mL), with Fe₃O₄ as the primary corrosion product ($\Delta V = 137.16$ mL) a 78 %
393 porosity loss can be expected. For all other oxide phases it is calculated that complete porosity
394 loss (100 %) will precede nano-Fe⁰ reactive exhaustion. However, in the practice a system
395 with 78 % porosity loss is considered as clogged. One possibility to avoid the clogging of the
396 entrance zone of a porous system is to intermittently inject calculated amounts of nano-Fe⁰.
397 The volume to be injected at each event and the time scale between two injections are
398 necessarily determined by site specific characteristics (e.g. aquifer porosity, water flow rate).

399 **5 Discussion**

400 A primary reason behind the interest into the use of nano-Fe⁰ particles over $\mu\text{m-Fe}^0$ and mm-
401 Fe⁰ particles for water treatment is ascribed to a significant increase the materials efficiency
402 [11,12]. For example, as reported by Vodyanitskii [79], Kanel et al. [80] reported near-total
403 remediation of a 1 mg L⁻¹ As^V solution within only 10 min by a nano-Fe⁰ with a specific
404 surface of 24 m²/g, whereas the same goal was achieved by mm-Fe⁰ (1–2 m²/g) after only 4
405 days or 5760 min (ratio of time 570; average ratio of surface 16). However, this experimental
406 evidence is highly qualitative as neither the number of atoms directly accessible at the surface
407 nor the intrinsic reactivity of individual materials are considered in both cases [34]. For a
408 better comparative result, the following three key conditions must be considered: (i) the
409 intrinsic Fe⁰ reactivity should be characterized, (ii) the amount of used materials should be
410 based on the reaction stoichiometry, and (iii) the experimental conditions should be relevant
411 for field applications. In particular, the driving force for the transport of contaminants and Fe

412 species should be relevant for field situations: (i) mixing operation (type and intensity) in
413 batch studies, (ii) flow rate and column dimensions in column studies [63].

414 **5.1 Transport of nano-Fe⁰ to the contaminants**

415 The efficiency of nano-Fe⁰ for the in-situ treatment of a contaminated aquifer body is
416 intrinsically linked to the extent of physical contact between Fe⁰ and any aqueous
417 contaminant species present. In some circumstances, contaminants could diffuse to the
418 suspended Fe⁰ particles and be degraded in the aqueous phase. However, typically the
419 suspended Fe⁰ particles must migrate to the contaminants. As Fe⁰ particles are transported
420 from the injection zone to the target contaminant plume by natural groundwater, diffusion
421 experiments under relevant groundwater velocity, using site specific aquifer materials are
422 essential in order to effectively assess the suitability of nano-Fe⁰ for in-situ applications [81].

423 Contaminants are typically partitioned between sediment and water phases in a “pseudo-
424 equilibrium” state. Therefore, it is likely that Fe⁰ particles whilst acting to reduce any soluble
425 contaminants are also likely to promote the dissolution of a range of adsorbed chemical
426 species (Le Chatelier’s principle). However, as water is also a redox-amenable species the
427 specific mechanism for nano-Fe⁰ reactivity in a range of conditions is difficult to resolve [30].
428 In other words, nano-Fe⁰ is readily oxidized by H₂O during subsurface migration to the target
429 contaminant plume and also competes with any other redox-amenable (including
430 contaminants) present in the groundwater. Additionally, expansive iron corrosion will yield
431 voluminous iron (hydr)oxides (Tab. 7) with limited aqueous mobility due to (i) an increased
432 size and weight, and (ii) a possible increased affinity to aquifer material.

433 This discussion has intentionally neglected the segregation between parent compounds, the
434 reaction products and their relative affinity to Fe⁰ and Fe (hydro)oxides. The fact that the core
435 Fe⁰ is always covered by oxide layers is also neglected for simplification. The process of
436 preferential flow which is crucial in predicting mass transfer in the subsurface is also not
437 considered [82-84]. However, it is clearly shown, that due the acute redox sensitivity of nano-

438 Fe^0 and the subsequent significant formation of highly voluminous oxidative corrosion
439 products it is likely that for environmentally relevant distances (m), a significant proportion of
440 the originally injected nano- Fe^0 will remain “clogged” in pore spaces.

441 Beside the transport of nano- Fe^0 to contaminants, the possibility of quantitative contaminant
442 desorption and their subsequent transformation by suspended Fe^0 could be considered.
443 However, it is not likely that concentration-gradient-driven mass transfer could be
444 quantitative at considered distances (m). It should be recalled that the slow kinetics of
445 contaminant desorption from aquifer materials is the major cause of the ineffectiveness of the
446 pump-and-treat technology for groundwater remediation [87-89].

447 This section has shown that it is likely that the success of nano- Fe^0 for in-situ remediation is
448 seriously limited by the intrinsic formation of voluminous iron corrosion products
449 [11,12,30,39,40]. Bearing this in mind, the next section suggests an alternative nano- Fe^0
450 subsurface deployment mechanism that more effectively takes into account the
451 aforementioned nano- Fe^0 hydraulic mobility issues than conventional injection processes: the
452 formation of a nano- Fe^0 “redox-front” injection array system for progressive contaminant
453 reduction. The geochemical process of redox-front migration is a well-documented one
454 [83,90,91].

455 **5.2 Nano- Fe^0 as source of Fe^{II} for a redox-front?**

456 **5.2.1 The concept**

457 The progressive consumption of mm- Fe^0 (Fig. 1; Tab. 3) is the guarantee for the long-term
458 efficiency of reactive barriers [11]. In fact, continuously generated small amount of high
459 reactive iron minerals [36,52-54,92-95] are sufficient for the removal of contaminants which
460 are present in trace amounts [96]. As discussed above, for nano- Fe^0 however, (i) Fe^0 reactive
461 exhaustion typically occurs in a relatively short time scale (< 9 hours) and, (ii) it is likely that
462 nano- Fe^0 subsurface mobility is significantly retarded or even prevented due to the volumetric
463 expansive nature of iron corrosion [46]. As a consequence an alternative method of

464 subsurface deployment is suggested in the current work: the deployment of a linear nano-Fe⁰
465 injection array orientated perpendicular to the flow direction of the contaminant plume. The
466 injected nano-Fe⁰ can effectively form a redox-front (roll-front) which migrates through the
467 contaminated zone and transforms the contaminants during its migration as illustrated in Fig.
468 5. The Fe^{II}/Fe^{III} roll-front travels across the contaminated zone with all possible mechanisms
469 (e.g. diffusion, dispersion, convection, preferential flow) and the contaminants are
470 transformed and immobilized during the cycle Fe^{II} ⇌ Fe^{III}. In other words, it is a plume of
471 Fe^{II}/Fe^{III} formed from injected nano-Fe⁰ which migrates through the contaminated zone and
472 “sweeps” the contaminants. As a consequence this method considers all nano-Fe⁰ mobility
473 issues.

474 **5.2.2 Nano-Fe⁰ as Fe^{II} generator**

475 Nano-Fe⁰ in the aqueous phase is certainly a Fe^{II}/Fe^{III} producer. Fe^{II}-species are the main
476 reducing agents for contaminants under both anoxic and oxic conditions [62]. The reducing
477 capacity of Fe^{II}-species nominally depends on the pH value [54,77,97,98]. Microbial activity
478 could regenerate Fe^{II} (bio-corrosion) for more contaminant reduction [79]. In this case, more
479 contaminant is reduced than can be predicted from the reaction stoichiometry. In order words,
480 the operating mode of nano-Fe⁰ for contaminant reduction can be summarized as follows: (i)
481 Fe⁰ is oxidized to produce Fe^{II}, (ii) Fe^{II} reduces the contaminant and is oxidized to Fe^{III}, and
482 (iii) a proportion of Fe^{II} is regenerated by the biological reduction of Fe^{III}. Accordingly,
483 before Fe⁰ depletion, there are three sources of Fe^{II}: (i) the Fe⁰ mediated abiotic oxidation by
484 H₂O, (ii) the Fe⁰ mediated abiotic oxidation by Fe^{III}, and (iii) the biological reduction of Fe^{III}.
485 After Fe⁰ depletion, the only remaining source of Fe^{II} is the biological reduction of Fe^{III}.
486 Provided that the appropriate micro-organism species are present in the subsurface, this
487 process, however, could conceptually proceed for a significantly long time period [35].
488 Evidence suggests that such micro-organism colonies can be sustained by a consistent supply
489 of Fe^{II}, Fe^{III} and molecular hydrogen (H/H₂). Another further process that is worth noting is

490 the generation of atomic or molecular hydrogen (H/H_2) by Fe^0 mediated hydrolysis reactions,
491 which is likely to aid and the aforementioned biotic processes [35].

492 The abiotic conversion of Fe^{III} to Fe^{II} has been successfully utilised in the hydrometallurgy
493 industry, for example Lottering et al. [99] reported on the sustainable use of MnO_2 for the
494 abiotic regeneration of Fe^{III} for U^{IV} oxidation.

495 The fate of contaminant reduction products is discussed in the next section.

496 **5.3 Mechanism of contaminant removal by injected nano- Fe^0**

497 The successful application of nano- Fe^0 injection technology for in-situ remediation is highly
498 dependent on a comprehensive understanding of the fundamental processes governing the
499 processes of contaminant removal. The hitherto discussion has focused on reductive
500 transformations by nano- Fe^0 . However, contaminant reductive transformation is not a
501 guarantee for contaminant removal [52-54]. Additionally, certain reaction products are more
502 toxic than their parent compounds [100]. Accordingly, efforts have to be focused on the
503 specific mechanism of aqueous contaminant removal. Relevant removal processes include: (i)
504 adsorption, (ii) chemical precipitation, (iii) co-precipitation, (iv) size exclusion or straining,
505 and (v) volatilization [52-54,79,101-104]. Chemical precipitation is a characteristic of
506 inorganic compounds when the solubility limit is exceeded [101,102,105]. Volatilization is
507 subsequent to chemical transformation yielding gaseous species like AsH_3 , CH_4 , CO_2 , H_2 , N_2 .
508 In Fe^0 reactive barrier systems, contaminants are efficiently removed by the combination of
509 adsorption, co-precipitation and size exclusion within the engineered barrier [14,106]. As a
510 result the current discussion concentrates on such processes..

511 With Fe^0 ($< 1 m^2/g$) first transformed to voluminous hydroxides species ($> 100 m^2/g$) and
512 subsequently transformed to oxides ($< 40 m^2/g$), contaminant size exclusion (straining) is
513 driven by the dynamic cycle of expansion/compression accompanying the corrosion process
514 [14,107]. During these cycles contaminants are enmeshed and sequestered in a “matrix” of
515 iron corrosion products.

516 For conventional nano-Fe⁰ injection arrays, size exclusion may play an important role (i) in
517 proximity for Fe⁰ particles, and (ii) by reducing the pore space during expansive corrosion of
518 the materials. However, if roll-fronts are formed as discussed above, the extent of
519 permeability loss in aquifer will be limited. The roll-front could act as a colloidal reactive
520 barrier for the removal of parent contaminants and reaction products. Species are removed or
521 immobilized by colloids and not because they are reduced. More research is needed to test
522 this hypothesis.

523 **5.3.1 Fe^{II}/Fe^{III} redox-front as a colloidal reactive barrier**

524 Aqueous contaminants have been reported to be quantitatively removed both during abiotic
525 and biotic (i) oxidation of Fe^{II} and (ii) reduction of Fe^{III} [107-109]. On the other hand,
526 injection of Fe^{III} salts for adsorptive contaminant removal has been reported [110,111].
527 Accordingly, the migration of the Fe^{II}/Fe^{III}-redox-front may be coupled to quantitative
528 contaminant removal by adsorption and co-precipitation.

529 The primary reason for contaminant removal during these redox reactions is the colloidal
530 nature of in-situ generated Fe species [Fe(OH)₂, Fe(OH)₃] [112], which necessarily
531 experience volumetric contraction to form oxides (of Fe^{II} or Fe^{III}). Contaminants are first
532 adsorbed by highly reactive colloids and are co-precipitated during transformation to
533 amorphous and crystalline oxides [79,113]

534 **6 Concluding remarks**

535 Constructed geochemical barriers of metallic iron (Fe⁰) have been used for groundwater
536 remediation since 1996 [1,5,6,79,114]. In recent years, however, nano-Fe⁰ has received
537 proclaim as a new tool for water treatment due to (i) improvements in reactivity and
538 associated aqueous contaminant removal performance compared to conventional materials,
539 and (ii) the option of subsurface deployment via injection for targeted in-situ treatment of
540 contaminant plumes [11,12].

541 Considering reactivity first, the current work has highlighted the need for prudent use of
542 terminology. Discounting any quantum size effects, which are only prevalent for Fe⁰ less than
543 approximately 10 nm in diameter, the reactivity of nano-Fe⁰ as a function of surface area is no
544 more reactive than larger forms. Nano-Fe⁰ only exhibits such high reactivity due to its
545 significantly high surface area as a function of mass/volume. Despite this, a recent trend in
546 research has been the development of bimetallic nano-Fe⁰ wherein the combination of a noble
547 metal acts to further increase the reactivity of nano-Fe⁰. It is argued in the current work that as
548 reactive exhaustion is already achieved by monometallic nano-Fe⁰ in the order of minutes this
549 seems counterintuitive for the majority of environmental applications.

550 Considering the nano-Fe⁰ subsurface injection procedure, in the current work it has been
551 highlighted that the hydraulic mobility of the particles is likely to be significantly retarded by
552 voluminous expansion due to particle corrosion. An alternative nano-Fe⁰ injection procedure
553 has been suggested herein. The injected nano-Fe⁰ effectively forms an in-situ migrating front
554 which possibly reductively transforms contaminant and removes reduced species by
555 adsorption and co-precipitation.

556 It is also outlined in the current work that a number of studies with experiments "proclaimed"
557 as analogous to environmental systems are largely overlooked a range of operational drivers
558 including changes in nano-Fe⁰ (i) reactivity, and (ii) voluminous as a function of time. It is
559 hoped that the huge literature on redox-front migration [115-118] and the cycle of iron in the
560 hydrosphere ([79] and ref. therein) will now be used for the further development of nano-Fe⁰
561 injection technology.

562 **Acknowledgments**

563 Mohammad A. Rahman (Angewandte Geologie - Universität Göttingen) is acknowledged for
564 technical support.

565 **Cited References**

- 566 [1] R.W. Gillham, S.F O'Hannesin, Enhanced degradation of halogenated aliphatics by zero-
567 valent iron, *Ground Water* 32 (1994) 958–967.
- 568 [2] L.J. Matheson, P.G. Tratnyek, Reductive dehalogenation of chlorinated methanes by iron
569 metal, *Environ. Sci. Technol.* 28 (1994) 2045–2053.
- 570 [3] D.W. Blowes, C.J. Ptacek, J.L. Jambor, In-situ remediation of Cr(VI)-contaminated
571 groundwater using permeable reactive walls: laboratory studies, *Environ. Sci. Technol.*
572 31 (1997) 3348–3357.
- 573 [4] S.F. O'Hannesin, R.W. Gillham, Long-term performance of an in situ "iron wall" for
574 remediation of VOCs, *Ground Water* 36 (1998) 164–170.
- 575 [5] M.M. Scherer, S. Richter, R.L. Valentine, P.J.J. Alvarez, Chemistry and microbiology of
576 permeable reactive barriers for in situ groundwater clean up, *Rev. Environ. Sci.*
577 *Technol.* 30 (2000) 363–411.
- 578 [6] A.D. Henderson, A.H. Demond, Long-term performance of zero-valent iron permeable
579 reactive barriers: a critical review, *Environ. Eng. Sci.* 24 (2007) 401–423.
- 580 [7] G. Bartzas, K. Komnitsas, Solid phase studies and geochemical modelling of low-cost
581 permeable reactive barriers, *J. Hazard. Mater.* 183 (2010) 301–308.
- 582 [8] Li L., Benson C.H., Evaluation of five strategies to limit the impact of fouling in
583 permeable reactive barriers, *J. Hazard. Mater.* 181 (2010) 170–180.
- 584 [9] C. Noubactep, S. Caré, Dimensioning metallic iron beds for efficient contaminant
585 removal, *Chem. Eng. J.* 163 (2010) 454–460.
- 586 [10] J.Y. Kim, H.-J. Park, C. Lee, K.L. Nelson, D.L. Sedlak, J. Yoon, Inactivation of
587 *Escherichia coli* by nanoparticulate zerovalent iron and ferrous ion, *Appl. Environ.*
588 *Microbiol.* 76 (2010) 7668–7670.

- 589 [11] S. Comba, A. Di Molfetta, R. Sethi, A comparison between field applications of nano-,
590 micro-, and millimetric zero-valent iron for the remediation of contaminated aquifers,
591 *Water Air Soil Pollut.* 215 (2011) 595–607.
- 592 [12] M. Gheju, Hexavalent chromium reduction with zero-valent iron (ZVI) in aquatic
593 systems, *Water Air Soil Pollut.* (2011) doi 10.1007/s11270-011-0812-y.
- 594 [13] S.-W. Jeon, R.B. Gillham, A. Przepiora, Predictions of long-term performance of
595 granular iron permeable reactive barriers: Field-scale evaluation, *J. Contam. Hydrol.*
596 123 (2011) 50–64.
- 597 [14] C. Noubactep, Metallic iron for safe drinking water production, *Freiberg Online*
598 *Geology*, 27 (2011) 38 pp, ISSN 1434-7512. (www.geo.tu-freiberg.de/fog)
- 599 [15] C.-B. Wang, W.-x. Zhang, Synthesizing nanoscale iron particles for rapid and complete
600 dechlorination of TCE and PCBs, *Environ. Sci. Technol.* 31 (1997) 2154–2156.
- 601 [16] S.M. Ponder, J.G. Darab, T.E. Mallouk, Remediation of Cr(VI) and Pb(II) aqueous
602 solutions using supported, nanoscale zero-valent iron, *Environ. Sci. Technol.* 34 (2000)
603 2564–2569.
- 604 [17] R. Muftikian, Q. Fernando, N. Korte, A method for the rapid dechlorination of low
605 molecular weight chlorinated hydrocarbons in water, *Water Res.* 29 (1995) 2434–2439.
- 606 [18] N.E. Korte, J.L. Zutman, R.M. Schlosser, L. Liang, B. Gu, Q. Fernando, Field
607 application of palladized iron for the dechlorination of trichloroethene, *Waste Manage.*
608 20 (2000) 687–694.
- 609 [19] B. Schrick, J.L. Blough, A.D. Jones, T.E. Mallouk, Hydrodechlorination of
610 trichloroethylene to hydrocarbons using bimetallic nickel–iron nanoparticles. *Chem.*
611 *Mater.* 14 (2002) 5140–5147.
- 612 [20] B. Karn, T. Kuiken, M. Otto, Nanotechnology and in situ remediation: A review of the
613 benefits and potential risks. *Environ. Health Perspectives* 117 (2009) 1832–1831.

- 614 [21] V. Nagpal, A.D. Bokare, R.C. Chikate, C.V. Rode, K.M. Paknikar, Reductive
615 dechlorination of γ -hexachlorocyclohexane using Fe–Pd bimetallic nanoparticles, J.
616 Hazard. Mater. 175 (2010) 680–687.
- 617 [22] K.-F. Chen, S. Li, W.-x. Zhang, Renewable hydrogen generation by bimetallic zerovalent
618 iron nanoparticles, Chem. Eng. J. (2011), doi:10.1016/j.cej.2010.12.019.
- 619 [23] S. Mossa Hosseini, B. Ataie-Ashtiani, M. Kholghi, Nitrate reduction by nano-Fe/Cu
620 particles in packed column, Desalination (2011) doi:10.1016/j.desal.2011.03.051.
- 621 [24] W.-X. Zhang, C.-B. Wang, H.-L. Lien, Treatment of chlorinated organic contaminants
622 with nanoscale bimetallic particles, Catal. Today 40 (1998) 387–395.
- 623 [25] R.W. Gillham, Discussion of Papers/Discussion of nano-scale iron for dehalogenation.
624 by Evan K. Nyer and David B. Vance (2001), Ground Water Monitoring &
625 Remediation, v. 21, no. 2, pages 41–54, Ground Water Monit. Remed 23 (2003) 6–8.
- 626 [26] W.-x. Zhang, Nanoscale iron particles for environmental remediation: an overview, J.
627 Nanopart. Res. 5 (2003) 323–332.
- 628 [27] X.Q. Li, D.W. Elliott, W.X. Zhang, Zero-valent iron nanoparticles for abatement of
629 environmental pollutants: materials and engineering aspects, Crit. Rev. Solid State
630 Mater. Sci. 31 (2006) 111–122.
- 631 [28] C. Macé, Controlling groundwater VOCs: do nanoscale ZVI particles have any
632 advantages over microscale ZVI or BNP? Pollut. Eng. 38 (2006) 24–27.
- 633 [29] C. Macé, S. Desrocher, F. Gheorghiu, A. Kane, M. Pupeza, M. Cernik, P. Kvapil, R.
634 Venkatakrishnan, W.-X. Zhang, Nanotechnology and groundwater remediation: A step
635 forward in technology understanding, Remed. J. 16 (2006) 23–33.
- 636 [30] P.G. Tratnyek, R.L. Johnson, Nanotechnologies for environmental cleanup, Nano Today
637 1 (2006) 44–48.
- 638 [31] T. Pradeep, Anshup, Noble metal nanoparticles for water purification: A critical review,
639 Thin Solid Films 517 (2009) 6441–6478.

- 640 [32] A. Agarwal, H. Joshi, Environmental sciences application of nanotechnology in the
641 remediation of contaminated groundwater: A short review, *Recent Res. Sci. Technol.* 2
642 (2010) 51–57.
- 643 [33] N. Müller, B. Nowack, Nano zero valent iron – THE solution for water and soil
644 remediation?. Report of workshop held in Zurich (Switzerland), November 24th 2009
645 (2010), http://www.observatorynano.eu/project/filesystem/files/nZVI_final_vsObservatory.pdf. (Access 2011/04/24)
- 646 [34] C. Noubactep, S. Caré, On nanoscale metallic iron for groundwater remediation, *J.*
647 *Hazard. Mater.* 182 (2010) 923–927.
- 648 [35] L.G. Cullen, E.L. Tilston, G.R. Mitchell, C.D. Collins, L.J. Shaw, Assessing the impact
649 of nano- and micro-scale zerovalent iron particles on soil microbial activities: Particle
650 reactivity interferes with assay conditions and interpretation of genuine microbial
651 effects, *Chemosphere* 82 (2011) 1675–1682.
- 652 [36] C. Noubactep, Comment on “Reductive dechlorination of g-hexachloro-cyclohexane
653 using Fe–Pd bimetallic nanoparticles” by Nagpal et al. [*J. Hazard. Mater.* 175 (2010)
654 680–687], *J. Hazard. Mater.* (2011) doi:10.1016/j.jhazmat.2011.03.081.
- 655 [37] J.R. Peralta-Videa, L. Zhao, M.L. Lopez-Moreno, G. de la Rosa, J. Hong, J.L. Gardea-
656 Torresdey, *Nanomaterials and the environment: A review for the biennium 2008–2010*,
657 *J. Hazard. Mater.* 186 (2011) 1–15.
- 658 [38] Z. Shi, J.T. Nurmi, P.G. Tratnyek, Effects of nano zero-valent iron on oxidation-
659 reduction potential, *Environ. Sci. Technol.* 45 (2011) 1586–1592.
- 660 [39] M.J. Truex, V.R. Vermeul, D.P. Mendoza, B.G. Fritz, R.D. Mackley, M. Oostrom, T.W.
661 Wietsma, T.W. Macbeth, Injection of zero-valent iron into an unconfined aquifer using
662 shear-thinning fluids, *Ground Water Monit. Remed.* 31 (2011) 50–58.
- 663 [40] M.J. Truex, T.W. Macbeth, V.R. Vermeul, B.G. Fritz, D.P. Mendoza, R.D. Mackley,
664 T.W. Wietsma, G. Sandberg, T. Powell, J. Powers, E. Pitre, M. Michalsen, S.J. Ballock-
665 Dixon, L. Zhong, M. Oostrom, Demonstration of combined zero-valent iron and

666 electrical resistance heating for in situ trichloroethene remediation. Environ. Sci.
667 Technol. (2011) doi: 10.1021/es104266a.

668 [41] T. Masciangioli, W.X. Zhang, Environmental technologies at the Nanoscale, Environ.
669 Sci. Technol. 37 (2003) 102A–108A.

670 [42] A. Ghauch, A. Tuqan, H. Abou Assi, Antibiotic removal from water: Elimination of
671 amoxicillin and ampicillin by microscale and nanoscale iron particles, Environ. Pollut.
672 157 (2009) 1626–1635.

673 [43] N. Sakulchaicharoen, D.M. O'Carroll, J.E. Herrera, Enhanced stability and dechlorination
674 activity of pre-synthesis stabilized nanoscale FePd particles, J. Contam. Hydrol. 118
675 (2010) 117–127.

676 [44] V. Nagpal, A.D. Bokare, R.C. Chikate, C.V. Rode, K.M. Paknikar, Reply to comment on
677 “Reductive dechlorination of γ -hexachlorocyclohexane using Fe–Pd bimetallic
678 nanoparticles”, by C. Noubactep, J. Hazard. Mater. (2011)
679 doi:10.1016/j.jhazmat.2011.04.015.

680 [45] C. Anstice, C. Alonso, F.J. Molina, Cover cracking as a function of bar corrosion: part I-
681 experimental test, Materials and structures 26 (1993) 453–464.

682 [46] S. Caré, Q.T. Nguyen, V. L'Hostis, Y. Berthaud, Mechanical properties of the rust layer
683 induced by impressed current method in reinforced mortar, Cement Concrete Res. 38
684 (2008) 1079–1091.

685 [47] Y. Zhao, H. Ren, H. Dai, W. Jin, Composition and expansion coefficient of rust based on
686 X-ray diffraction and thermal analysis, Corros. Sci. 53 (2011) 1646–1658.

687 [48] K.D. Grieger, A. Fjordboge, N.B. Hartmann, E. Eriksson, P.L. Bjerg, A. Baun,
688 Environmental benefits and risks of zero-valent iron nanoparticles (nZVI) for in situ
689 remediation: Risk mitigation or trade-off? J. Contam. Hydrol. 118 (2010) 165–183.

- 690 [49] R.J. Barnes, C. J. van der Gast, O. Riba, L.E. Lehtovirta, J.I. Prosser, P.J. Dobson, I.P.
691 Thompson, The impact of zero-valent iron nanoparticles on a river water bacterial
692 community, *J. Hazard. Mater.* 184 (2010) 73–80.
- 693 [50] M. Diao, M. Yao, Use of zero-valent iron nanoparticles in inactivating microbes, *Water*
694 *Res.* 43 (2009) 5243–5251.
- 695 [51] T. Tervonen, I. Linkov, J.R. Figueira, J. Steevens, M. Chappell, M. Merad, Risk-based
696 classification system of nanomaterials, *J. Nanopart. Res.* 11 (2009) 757–766.
- 697 [52] C. Noubactep (2007): Processes of contaminant removal in “Fe⁰-H₂O” systems revisited.
698 The importance of co-precipitation, *Open Environ. J.* 1, 9–13.
- 699 [53] C. Noubactep A critical review on the mechanism of contaminant removal in Fe⁰-H₂O
700 systems, *Environ. Technol.* 29 (2008) 909–920.
- 701 [54] C. Noubactep, The fundamental mechanism of aqueous contaminant removal by metallic
702 iron, *Water SA* 36 (2010) 663–670.
- 703 [55] M.I. Litter, M.E. Morgada, J. Bundschuh, Possible treatments for arsenic removal in
704 Latin American waters for human consumption, *Environ. Pollut.* 158 (2010) 1105–1118.
- 705 [56] R.A. Crane, M. Dickinson, I.C. Popescu, T.B. Scott, Magnetite and zero-valent iron
706 nanoparticles for the remediation of uranium contaminated environmental water, *Water*
707 *Res.* 45 (2011) 2931–2942.
- 708 [57] O. Celebi, C. Uzum, T. Shahwan, H.N. Erten, A radiotracer study of the adsorption
709 behavior of aqueous Ba²⁺ ions on nanoparticles of zero-valent iron, *J. Hazard. Mater.*
710 148 (2007) 761–767.
- 711 [58] X.Q. Li, W.X. Zhang, Sequestration of metal cations with zerovalent iron
712 nanoparticles—a study with high resolution X-ray photoelectron spectroscopy (HR-
713 XPS), *J. Phys. Chem. C* 111 (2007) 6939–6946.

- 714 [59] H.K. Boparai, M. Joseph, D.M. O'Carroll, Kinetics and thermodynamics of cadmium ion
715 removal by adsorption onto nano zerovalent iron particles, *J. Hazard. Mater.* 186 (2011)
716 458–465.
- 717 [60] S. Xiao, H. Ma, M. Shen, S. Wang, Q. Huang, X. Shi, Excellent copper(II) removal using
718 zero-valent iron nanoparticle - immobilized hybrid electrospun polymer nanofibrous
719 mats, *Colloids Surf. A: Physicochem. Eng. Aspects* 381 (2011) 48–54.
- 720 [61] E.J. Reardon, R. Fagan, J.L. Vogan, A. Przepiora, Anaerobic corrosion reaction kinetics
721 of nanosized iron, *Environ. Sci. Technol.* 42 (2008) 2420–2425.
- 722 [62] M. Stratmann, J. Müller, The mechanism of the oxygen reduction on rust-covered metal
723 substrates, *Corros. Sci.* 36 (1994) 327–359.
- 724 [63] C. Noubactep, T. Licha, T.B. Scott, M. Fall, M. Sauter, Exploring the influence of
725 operational parameters on the reactivity of elemental iron materials, *J. Hazard. Mater.*
726 172 (2009) 943–951.
- 727 [64] S.H. Behrens, D.I. Christl, R. Emmerzael, P. Schurtenberger, M. Borkovec, Charging
728 and aggregation properties of carboxyl latex particles: experiments versus DLVO
729 theory, *Langmuir* 21 (2000) 2566–2575.
- 730 [65] M. Dickinson, T.B. Scott, The application of zero-valent iron nanoparticles for the
731 remediation of a uranium-contaminated waste effluent, *J. Hazard. Mater.* 178 (2010)
732 171–179.
- 733 [66] R.L. Johnson, R.B. Thoms, R.O.B. Johnson, J. Nurmi, P.G. Tratnyek, Mineral
734 precipitation upgradient from a zero-valent iron permeable reactive barrier, *Ground*
735 *Water Monit. Rem.* 28 (2008) 56–64.
- 736 [67] Y. Wu, J. Zhang, Y. Tong, X. Xu, Chromium (VI) reduction in aqueous solutions by
737 Fe₃O₄-stabilized Fe⁰ nanoparticles, *J. Hazard. Mater.* 172 (2009) 1640–1645.

- 738 [68] Z. Fang, X. Qiu, J. Chen, X. Qiu, Degradation of the polybrominated diphenyl ethers by
739 nanoscale zero-valent metallic particles prepared from steel pickling waste liquor,
740 *Desalination* 267 (2011) 34–41.
- 741 [69] Z.LvL. Jiang, W. Zhang, Q. Du, B. Pan, L. Yang, Q. Zhang, Nitrate reduction using
742 nanosized zero-valent iron supported by polystyrene resins: Role of surface functional
743 groups. *Water Res.* 45 (2011) 2191–2198.
- 744 [70] M. Tong, S. Yuan, H. Long, M. Zheng, L. Wang, J. Chen, Reduction of nitrobenzene in
745 groundwater by iron nanoparticles immobilized in PEG/nylon membrane, *J. Contam.*
746 *Hydrol.* 122 (2011) 16–25.
- 747 [71] S. Yuan, Z. Zheng, X.-Z. Meng, J. Chen, L. Wang, Surfactant mediated HCB
748 dechlorination in contaminated soils and sediments by micro and nanoscale Cu/Fe
749 Particles. *Geoderma* 159 (2010) 165–173.
- 750 [72] N. Zhu, H. Luan, S. Yuan, J. Chen, X. Wu, L. Wang, Effective dechlorination of HCB by
751 nanoscale Cu/Fe particles. *J. Hazard. Mater.* 176 (2010), 1101–1105.
- 752 [73] B.S. Kadu, Y.D. Sathe, A.B. Ingle, R.C. Chikate, K.R. Patil, C.V. Rode, Efficiency and
753 recycling capability of montmorillonite supported Fe–Ni bimetallic nanocomposites
754 towards hexavalent chromium remediation, *Appl. Catal. B: Environ.* 104 (2011) 407–
755 414.
- 756 [74] C. Noubactep, S. Caré, F. Togue-Kamga, A. Schöner, P. Woafu, Extending service life
757 of household water filters by mixing metallic iron with sand, *Clean – Soil, Air, Water* 38
758 (2010) 951–959.
- 759 [75] V. Tarvainen, A. Ranta-Maunus, A. Hanhijärvi, H. Forsén, The effect of drying and
760 storage conditions on case hardening of scots pine and norway spruce timber, *Maderas.*
761 *Ciencia y tecnología* 8 (2006) 3–14.

- 762 [76] W.J.N. Fernando, A.L. Ahmad, S.R. Abd. Shukor, Y.H. Lok, A model for constant
763 temperature drying rates of case hardened slices of papaya and garlic, *J. Food Eng.* 88
764 (2008) 229–238
- 765 [77] Y. Zhuang, S. Ahn, A.L. Seyfferth, Y. Masue-Slowey, S. Fendorf, R.G. Luthy,
766 Dehalogenation of polybrominated diphenyl ethers and polychlorinated biphenyl by
767 bimetallic, impregnated, and nanoscale zerovalent iron, *Environ. Sci. Technol.* 45
768 (2011) 4896–4903.
- 769 [78] N. Moraci, P.S. Calabrò, Heavy metals removal and hydraulic performance in zero-
770 valent iron/pumice permeable reactive barriers, *J. Environ. Manag.* 91 (2010) 2336–
771 2341.
- 772 [79] Y.N. Vodyanitskii, The role of iron in the fixation of heavy metals and metalloids in
773 soils: a review of publications, *Eurasian Soil Sci.* 43 (2010) 519–532.
- 774 [80] S.R. Kanel, J.-M. Greneche, H. Choi, Arsenic(V) Removal from groundwater using nano
775 scale zero-valent iron as a colloidal reactive barrier material, *Environ. Sci. Technol.* 40
776 (2006) 2045–2050.
- 777 [81] D.D.J. Antia, Modification of aquifer pore-water by static diffusion using nano-zero-
778 valent metals. *Water* 3 (2011) 79–112.
- 779 [82] M. Flury, H. Flühler, Brilliant Blue FCF as a dye tracer for solute transport studies. A
780 toxicological review, *J. Environ. Qual.* 23 (1994) 1108–1112.
- 781 [83] A.E. Fryar, F.W. Schwartz, Hydraulic-conductivity reduction, reaction-front propagation,
782 and preferential flow within a model reactive barrier, *J. Contam. Hydrol.* 32 (1998) 333–
783 351.
- 784 [84] J. Simunek, N.J. Jarvis, M.T. van Genuchten, A. Gardenas, Review and comparison of
785 models for describing non-equilibrium and preferential flow and transport in the vadose
786 zone, *J. Hydrol.* 272 (2003) 14–35.

- 787 [85] B.E. Clothier, S.R. Green, M. Deurer, Preferential flow and transport in soil: progress
788 and prognosis, *Eur. J. Soil Sci.* 59 (2008) 2–13.
- 789 [86] S.E. Allaire, S. Roulier, A.J. Cessna, Quantifying preferential flow in soils: A review of
790 different techniques, *J. Hydrol.* 378 (2009) 179–204.
- 791 [87] D.C. McMurty, R.O. Elton, New approach to in-situ treatment of contaminated
792 groundwaters, *Environ. Progr.* 4/3 (1985) 168–170.
- 793 [88] M.D. Mackay, J.A. Cherry, Groundwater contamination: Pump-and-treat remediation,
794 *Environ. Sci. Technol.* 23 (1989) 630–636.
- 795 [89] R.C. Starr, J.A. Cherry, In situ remediation of contaminated Ground water: The funnel-
796 and-Gate System, *Ground Water* 32 (1994) 465–476.
- 797 [90] M. Min, H. Xu, J. Chen, M. Fayek, Evidence of uranium biomineralization in sandstone-
798 hosted roll-front uranium deposits, northwestern China, *Ore Geol. Rev.* 26 (2005) 198–
799 206.
- 800 [91] M. Sidborn, I. Neretnieks, Long term redox evolution in granitic rocks: Modelling the
801 redox front propagation in the rock matrix, *Appl. Geochem.* 22 (2007) 2381–2396.
- 802 [92] B. Gu, T.J. Phelps, L. Liang, M.J. Dickey, Y. Roh, B.L. Kinsall, A.V. Palumbo, G.K.
803 Jacobs, Biogeochemical dynamics in zerovalent iron columns: implications for
804 permeable reactive barriers, *Environ. Sci. Technol.* 33 (1999) 2170–2177.
- 805 [93] C. Su, R.W. Puls, Arsenate and arsenite removal by zerovalent iron: kinetics, redox
806 transformation, and implications for in situ groundwater remediation, *Environ. Sci.*
807 *Technol.* 35 (2001) 4562–4568.
- 808 [94] Y. Furukawa, J.-W. Kim, J. Watkins, R.T. Wilkin, Formation of ferrihydrite and
809 associated iron corrosion products in permeable reactive barriers of zerovalent iron,
810 *Environ. Sci. Technol.* 36 (2002) 5469–5475.

- 811 [95] T. Kohn, J.T. Kenneth, A. Livi, A.L. Roberts, P.J. Vikesland, Longevity of granular iron
812 in groundwater treatment processes: corrosion product development, *Environ. Sci.*
813 *Technol.* 39 (2005) 2867–2879.
- 814 [96] C.D. Palmer, P.R. Wittbrodt, Processes affecting the remediation of chromium-
815 contaminated sites, *Environ. Health Perspect.* 92 (1991) 25–40.
- 816 [97] S. Nestic, Key issues related to modelling of internal corrosion of oil and gas pipelines –
817 A review, *Corros. Sci.* 49 (2007) 4308–4338.
- 818 [98] J.R. Kiser, Bruce A. Manning, Reduction and immobilization of chromium(VI) by
819 iron(II)-treated faujasite. *J. Hazard. Mater.* 174 (2010) 167–174.
- 820 [99] M.J. Lottering, L. Lorenzen, N.S. Phala, J.T. Smit, G.A.C. Schalkwyk, Mineralogy and
821 uranium leaching response of low grade South African ores, *Miner. Eng.* 21 (2008) 16–
822 22.
- 823 [100] Y. Jiao, C. Qiu, L. Huang, K. Wu, H. Ma, S. Chen, L. Ma, L. Wu, Reductive
824 dechlorination of carbon tetrachloride by zero-valent iron and related iron corrosion,
825 *Appl. Catal. B: Environ.* 91 (2009) 434–440.
- 826 [101] R.J. Crawford, I.H. Harding, D.E. Mainwaring, Adsorption and coprecipitation of single
827 heavy metal ions onto the hydrated oxides of iron and chromium, *Langmuir* 9 (1993)
828 3050–3056.
- 829 [102] R.J. Crawford, I.H. Harding, D.E. Mainwaring, Adsorption and coprecipitation of
830 multiple heavy metal ions onto the hydrated oxides of iron and chromium, *Langmuir* 9
831 (1993) 3057–3062.
- 832 [103] K. Eusterhues, T. Rennert, H. Knicker, I. Kgel-Knabner, K.U. Totsche, U.
833 Schwertmann, Fractionation of organic matter due to reaction with ferrihydrite:
834 Coprecipitation versus adsorption, *Environ. Sci. Technol.* 45 (2011) 527–533.

- 835 [104] W.P. Johnson, H. Ma, E. Pazmino, Straining credibility: A general comment regarding
836 common arguments used to infer straining as the mechanism of colloid retention in
837 porous media, *Environ. Sci. Technol.* 45 (2011) 3831–3832.
- 838 [105] M. Kalin, W.N. Wheeler, G. Meinrath, The removal of uranium from mining waste
839 water using algal/microbial biomass, *J. Environ. Radioact.* 78 (2005) 151–177.
- 840 [106] C. Noubactep, Metallic iron for safe drinking water worldwide, *Chem. Eng. J.* 165
841 (2010) 740–749.
- 842 [107] D. Pokhrel, T. Viraraghavan, Arsenic removal in an iron oxide-coated fungal biomass
843 column: Analysis of breakthrough curves, *Biores. Technol.* 99 (2008) 2067–2071.
- 844 [108] D. Pokhrel, B.S. Bhandari, T. Viraraghavan, Arsenic contamination of groundwater in
845 the Terai region of Nepal: an overview of health concerns and treatment options,
846 *Environ. Int.* 35 (2009) 157–161.
- 847 [109] D. Pokhrel, T. Viraraghavan, Biological filtration for removal of arsenic from drinking
848 water, *J. Environ. Manage.* 90 (2009) 1956–1961.
- 849 [110] J.S. Morrison, R.R. Sprangler, Chemical barriers for controlling groundwater
850 contamination, *Environ. Progr.* 12 (1993) 175–181.
- 851 [111] J.S. Morrison, R.R. Sprangler, S.A. Morris, Subsurface injection of dissolved ferric
852 chloride to form a chemical barrier: Laboratory investigations, *Ground Water* 34 (1996)
853 75–83.
- 854 [112] K. Hanna, J.-F. Boily, Sorption of two naphthoic acids to goethite surface under flow
855 through conditions, *Environ. Sci. Technol.* 44 (2010) 8863–8869.
- 856 [113] A. Ghauch, H. Abou Assi, S. Bdeir Aqueous removal of diclofenac by plated elemental
857 iron: Bimetallic systems, *J. Hazard. Mater.* 182 (2010) 64–74.
- 858 [114] C. Noubactep, Aqueous contaminant removal by metallic iron: Is the paradigm shifting?
859 *Water SA* 37 (2011) xy–zt.

- 860 [115] R.L. Reynolds, M.B. Goldhaber, Origin of a south Texas roll-type uranium deposit: I.
861 Alteration of iron-titanium oxide minerals, *Econ. Geol.* 73 (1978) 1677–1689.
- 862 [116] J. Posey-Dowty, E. Axtmann, D. Crerar, M. Borcsik, A. Ronk, W. Woods, Dissolution
863 rate of uraninite and uranium roll-front ores. *Econ. Geol.* 82 (1987) 184–194.
- 864 [117] L. Romero, I. Neretnieks, L. Moreno, Movement of the redox front at the Osamu
865 Utsumi uranium mine, Poços de Caldas, Brazil, *J. Geochem. Explor.* 45 (1992) 471–
866 501.
- 867 [118] D. Read, T.A. Lawless, R.J. Sims, K.R. Butter, Uranium migration through intact
868 sandstone cores, *J. Cont. Hydrol.*, 13 (1993) 277–289.
- 869

870 **Table 1:** Results of a web-search in 7 selected relevant journals demonstrating the current
 871 interest within academia for the nano-Fe⁰ technology.

872

873

Journal	Impact	Issues	Search's results		
	Factor	(year ⁻¹)	Period	Total	2011
Environ. Sci. Technol.	4.630	24	1995 to 2011	157	13
J. Hazard. Mater.	4.144	33	2004 to 2011	86	15
Chemosphere	3.253	44	2000 to 2011	49	5
Water Res.	4.355	20	2005 to 2011	31	9
Chem. Eng. J.	2.816	30	2008 to 2011	15	6
Desalination	2.034	48	2008 to 2011	12	9
Environ. Pollut.	3.426	12	2007 to 2011	12	1
Appl. Catal. B	5.252	32	2009 to 2011	3	1
Total				365	59

874

875 **Table 2:** Relevant redox couples for the process of aqueous Fe⁰ dissolution and oxide scale
 876 formation in a passive remediation Fe⁰/H₂O system. These processes are thermodynamically
 877 the same for all Fe⁰ particle sizes. Observed differences are due to kinetics aspects.
 878

Electrode reactions			Eq.
Fe ⁰	⇌	Fe ²⁺ + 2 e ⁻	(1)
Oxic conditions			
O ₂ + 2 H ₂ O + 4 e ⁻	⇌	4 OH ⁻	(2a)
2 H ₂ O + 2 e ⁻	⇌	H ₂ + 2 OH ⁻	(2b)
Anoxic conditions			
O ₂ + 4 H ⁺ + 4 e ⁻	⇌	2 H ₂ O	(3a)
2 H ⁺ + 2 e ⁻	⇌	H ₂	(3b)

879

880 **Table 3:** Summary of the values of the number of particles contained in 1 kg of each material,
881 the number of layer making up each particle and estimation of the relative time (τ).
882 The life span of nano-Fe⁰ is operationally considered as the unit of time while
883 assuming uniform corrosion. τ coincides with the ratio of the number of layers of Fe
884 in each particle to that of nano-Fe⁰. The ratio of the number of particles in individual
885 systems is also given.

886

Size	d	n _{particles}	n _{layers}	n _{layers} /n _{nano}	n _{nano} /n _{particles}	τ
	(μm)	(-)	(-)	(-)	(-)	(-)
Nano-Fe⁰	25*10 ⁻³	1.96*10 ¹⁸	87.2	1.0	1.0	1.0
$\mu\text{m-Fe}^0$	25	1.96*10 ⁹	87.2*10 ³	10 ³	10 ⁹	10 ³
mm-Fe⁰	250	1.96*10 ⁶	87.2*10 ⁴	10 ⁴	10 ¹²	10 ⁴
mm-Fe⁰	1000	3.06*10 ⁴	3.49*10 ⁵	4*10 ⁴	6.4*10 ¹³	4*10 ⁴

887

888

889

890 **Table 4:** Estimation of the value of the life span (t_{∞}) of a nano-Fe⁰ particle with 25 nm
 891 diameter for barrier life spans (t) from 10 to 40 years. The considered conventional reactive
 892 wall contains granular Fe⁰ with a diameter of 1 mm. For comparison the relative life span (in
 893 days and years) of the micrometric particles is given.

894

t	(years)	5	10	15	20	25	30	35	40
t_{μm}	(days)	45.7	91.3	137.0	182.6	228.3	273.9	319.6	365.3
t_{μm}	(years)	0.2	0.3	0.5	0.7	0.9	1.0	1.2	1.4
t_∞	(hours)	1.1	2.2	3.3	4.4	5.5	6.6	7.7	8.8

895

896

897

898 **Table 5:** Estimation of the extent of porosity loss (ΔV) due to the volumetric expansion of
 899 iron corrosion for Fe^0 particles of different sizes. The operational unit of time is
 900 arbitrarily the time to nano- Fe^0 depletion (t_∞). V_0 is the volume occupied by the
 901 initial Fe^0 particles; V_∞ is the volume occupied by residual Fe^0 and in-situ formed
 902 corrosion products. ΔV corresponds to the volume of pore occupied by the
 903 volumetric expansion of corrosion products. m_{consumed} = mass of Fe^0 consumed; v =
 904 percent of Fe^0 depletion, $n_{\text{Fe(II)}}$ = number of moles of corroded Fe^0 ; $n_{\text{Fe}_3\text{O}_4}$ = number
 905 of moles of generated iron corrosion products, $n_{\text{electrons}} = 2 * n_{\text{Fe(II)}}$ = number of
 906 electrons released by corroded iron; and $n_{\text{nano}}/n_{\text{electrons}}$ is the ratio of the number of
 907 electrons produced in by nano- Fe^0 to $n_{\text{electrons}}$.
 908

Size	m_{consumed}	v	V_∞	ΔV	ΔV	$n_{\text{Fe(II)}}$	$n_{\text{Fe}_3\text{O}_4}$	$n_{\text{electrons}}$	$n_{\text{nano}}/n_{\text{electrons}}$
	(kg)	(%)	(mL)	(mL)	(%)	(moles)	(moles)	(moles)	(-)
nm- Fe^0	10^0	100.00	264.16	137.16	108.00	17.857	5.9524	35.714	1
μm - Fe^0	$3 * 10^{-3}$	0.30	127.41	0.41	0.32	0.053	0.0178	0.107	335
mm- Fe^0	$3 * 10^{-4}$	0.03	127.04	0.04	0.03	0.005	0.0018	0.011	3342
mm- Fe^0	$7.5 * 10^{-5}$	0.01	127.01	0.01	0.01	0.001	0.0004	0.003	13369

909

910

911

912 **Table 6:** Summary of the values of the number of particles contained in 1 kg of each nano-
 913 Fe⁰, the number of layer making up each particle and estimation of the relative time
 914 (τ). The life span of the material with the smallest particle size ($d = 10$ nm) is
 915 operationally considered as the unit of time while assuming uniform corrosion. The
 916 ratio of the number of particles in 1 kg of $d = 10$ nm to that of other d values is also
 917 given.

918

d	n_{particles}	n_{layers}	n_{layers}/n₁₀	n₁₀/n_{particles}	τ
(nm)	(-)	(-)	(-)	(-)	(-)
10	3.06*10 ¹⁹	34.9	1.0	1.0	1.0
25	1.96*10 ¹⁸	87.2	2.5	16	2.5
50	2.45*10 ¹¹	174.5	5.0	125	5.0
75	7.25*10 ¹⁶	261.7	7.5	422	7.5
100	3.06*10 ¹⁶	348.9	10.0	1000	10.0

919

920

921 **Table 7:** Summary of the extent of porosity loss (ΔV_{pore} in %) as 1 kg of nano-Fe⁰ ($V_0 = 127$
922 mL) is corroded to various iron oxides. V_{∞} is the volume of iron oxide at Fe⁰
923 exhaustion. The initial volume of pore (V_{pore}) is 530.4 mL and V'_{pore} is the residual
924 pore volume at Fe⁰ exhaustion. The absolute value of negative values for V'_{pore}
925 corresponds to the mass of nano-Fe⁰ which can not oxidize because of lack of space
926 for volumetric expansion.

927

Fe species	η	V_{∞}	ΔV	V'_{pore}	ΔV_{pore}
	(-)	(mL)	(mL)	(mL)	(%)
Fe ⁰	1	127	0	403.4	23.9
Fe ₃ O ₄	2.08	264.2	137.2	266.2	49.8
Fe ₂ O ₃	2.12	269.2	142.3	261.1	50.8
α -FeOOH	2.91	369.6	242.6	160.8	69.7
γ -FeOOH	3.03	384.8	258.0	145.6	72.6
β -FeOOH	3.48	442.0	315.0	88.4	83.3
Fe(OH) ₂	3.75	476.3	349.3	54.1	89.8
Fe(OH) ₃	4.2	533.4	406.4	-3.0	100.0
Fe(OH) ₃ .3H ₂ O	6.4	812.8	685.8	-282.4	100.0

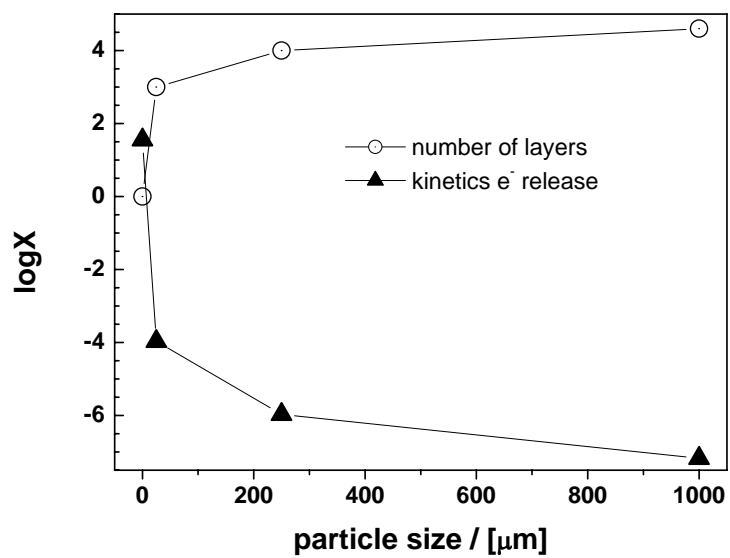
928

929

930

931 **Figure 1**

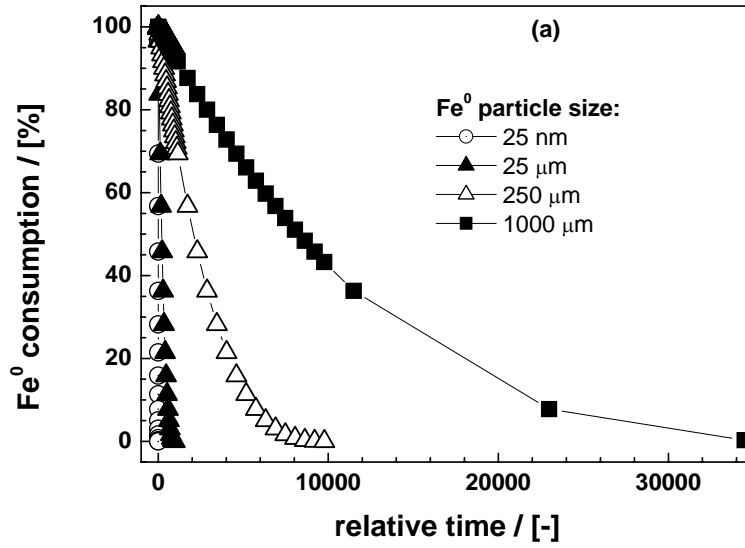
932



933

934 **Figure 2**

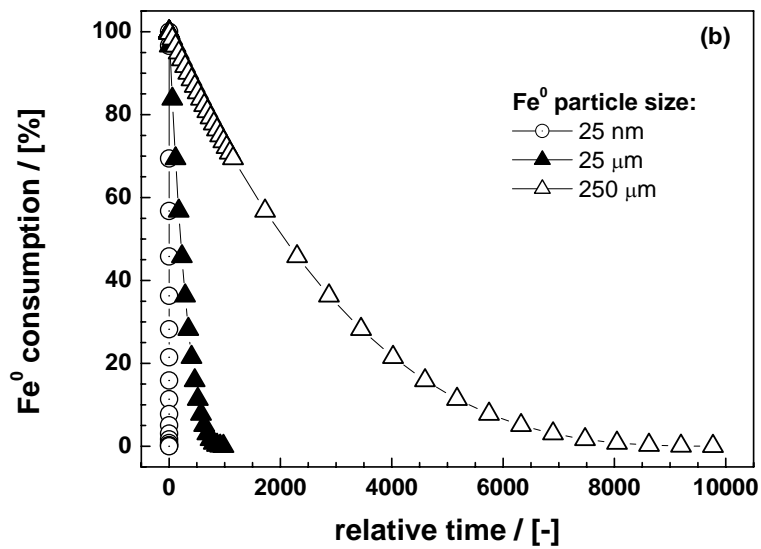
935



936

937

938



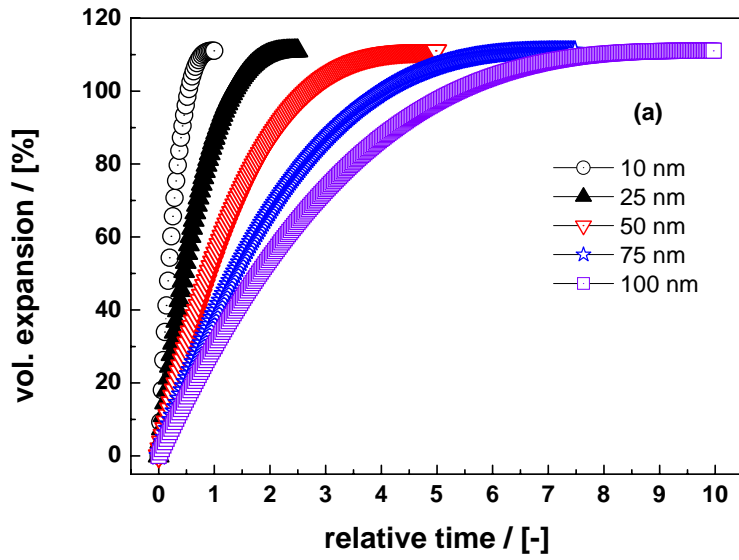
939

940

941 **Figure 3**

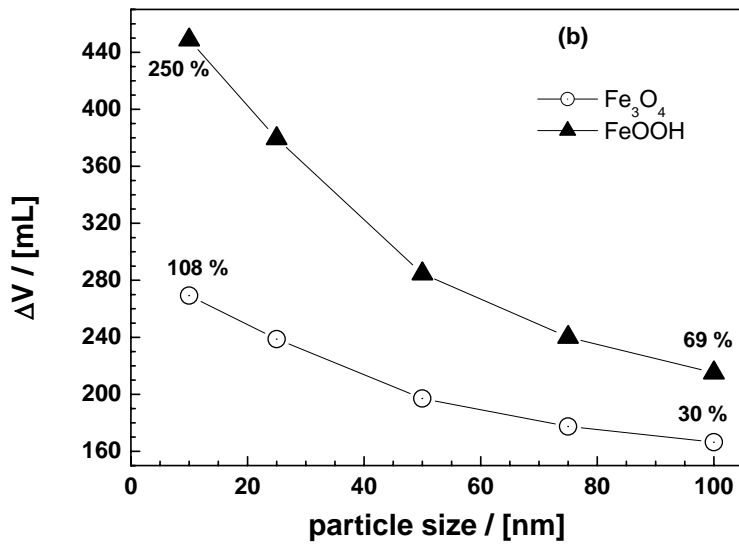
942

943



944

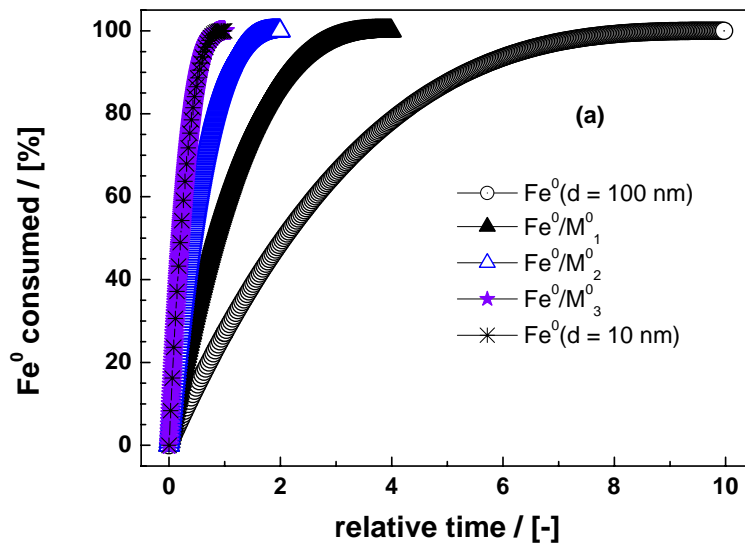
945



946

947 **Figure 4:**

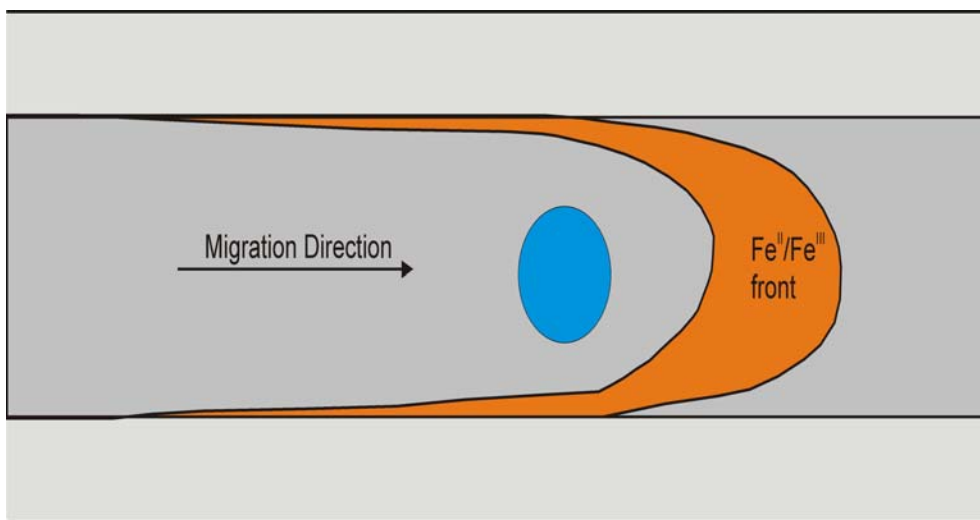
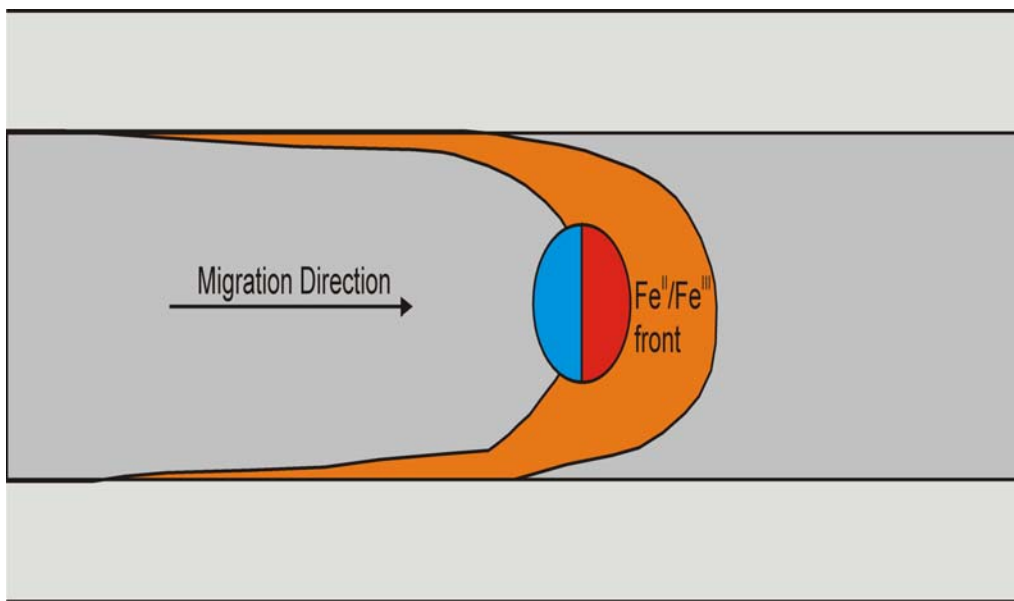
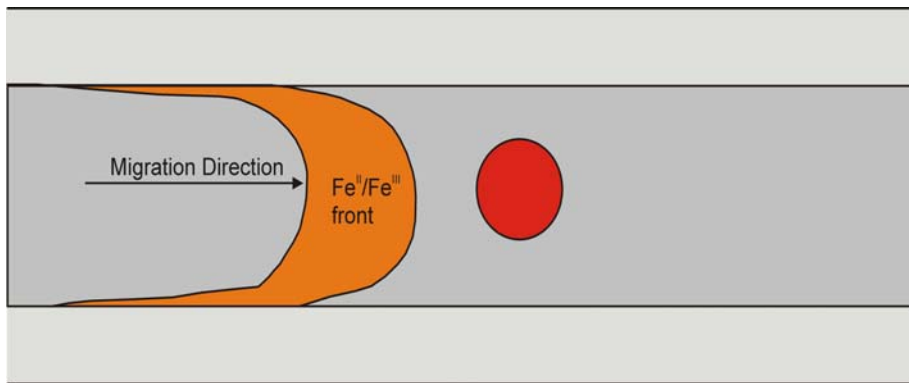
948



949

950

951 **Figure 5**



958 **Figure captions**

959

960 **Figure 1:** Comparison of the evolution of the kinetics of electron release and the number of
961 layers in each Fe^0 particle as a function of the particle size. It is shown that smaller particles
962 release huge amounts of electrons within a very short time. Calculations are made for 1 kg of
963 Fe^0 material.

964 **Figure 2:** Kinetics of the process of Fe^0 exhaustion at nano-, micro- and millimetre scale as
965 for: (a) $d \leq 1000 \mu\text{m}$, and (b) $d \leq 200 \mu\text{m}$.

966 **Figure 3:** Kinetics of the process of porosity loss at nano-scale as characterized by: (a) the
967 percent volumetric expansion for the five considered particle sizes, and (b) the absolute value
968 of ΔV (mL) at $\tau = 1$ for two different iron corrosion products (Fe_3O_4 and FeOOH).

969 **Figure 4:** Calculated extent of Fe^0 exhaustion as a function of the relative time (τ) for three
970 ideal bimetallic systems based on the material with 100 nm diameter. The material with 10
971 nm diameter is represented for comparison.

972 **Figure 5:** Schematic diagram of the flow process of the U-shaped redox-front through a
973 contaminated zone. Despite the relative importance of preferential flow paths, contaminants
974 are “swept” by the roll-front.

975

976